International Journal of Biological Macromolecules 180 (2021) 299–310

Contents lists available at ScienceDirect

International Journal of Biological Macromolecules

journal homepage: http://www.elsevier.com/locate/ijbiomac

Pretreatment of lignocellulosic waste as a precursor for synthesis of high porous activated carbon and its application for Pb (II) and Cr (VI) adsorption from aqueous solutions

Seyyedeh Maryam Kharrazi [a], Mohsen Soleimani [a], Mojtaba Jokar [a], Tobias Richards [b], Anita Pettersson [b], Nourollah Mirghaffari [a,*]

[a] Department of Natural Resources, Isfahan University of Technology, Isfahan 84156-83111, Iran
[b] Department of Resource Recovery and Building Technology, Faculty of Textiles, Engineering and Business, University of Borås, S-501 90 Borås, Sweden

ARTICLE INFO

Article history:
Received 28 December 2020
Received in revised form 27 February 2021
Accepted 13 March 2021
Available online 16 March 2021

Keywords:
Elm tree
Heavy metals
Chemical activation

ABSTRACT

Effects of Elm tree sawdust pretreatments using alkali and alkaline earth metals (NaCl, KCl, $CaCl_2$, $MgCl_2$ and Elm tree ash) and deashing solutions (water, HCl, HNO_3 and aqua regia) before the carbonization process on the porosity of produced activated carbons and Pb (II) and Cr (VI) adsorption were studied. The activated carbons were characterized by pore size distribution, surface area, FTIR, and SEM-EDX analyses. Based on the results, HCl leaching pretreatment of the biomass increased the activated carbon adsorption capacity of Cr (VI) from 114 to 190 mg g^{-1}. The treatment of biomass with alkali and alkali earth metal salts, especially $MgCl_2$, remarkably increased the activated carbon adsorption capacity of Pb (II) from 233 to 1430 mg g^{-1}. The results indicated that Pb (II) adsorption was attributed to both the mesoporous structure of activated carbon and the abundance of Mg on the activated carbon's surface. On the other hand, the micropores played a major role in Cr (VI) adsorption capacity. The development of the micro- or mesoporous structure of activated carbons through pretreatment of lignocellulosic precursor could be an approach for providing high performance activated carbons for Pb (II) and Cr (VI) removal from aqueous solutions.

1. Introduction

Activated carbon (AC) produced from thermal conversion of carbonaceous precursors has been extensively used in a wide range of applications such as removal of wastewater pollutants, electrode materials in supercapacitator, medical uses and gas storage [1]. A variety of biological wastes such as plant and agricultural residues, sludge, and animal wastes can be employed as a feedstock of carbonization process [2]. Today, there is a special focus on the use of different types of inexpensive biomass as sustainable sources of AC to remove mineral and organic contaminants from effluents [3–5]. One of the most available and low-cost carbonaceous materials which could be used as raw material for the production of AC are lignocellulosic wastes [6].

Due to industrialization and technological development, the release of heavy metals (e.g. lead (Pb), cadmium (Cd), chromium (Cr), nickel (Ni), arsenic (As), and mercury (Hg)) are highly concerned to the environment and public health due to their toxicity and accumulation in the food chain. Liver and kidney damage, anemia in low doses and carcinogenic effect in high concentrations are the most adverse outcomes of exposure to heavy metals [7]. Cr (VI) is a known human carcinogen that can enter the cell. It tends to form CrO_4^{2-} or $HCrO_4^-$ in the natural aqueous environment [8]. Pb (II) is a neurotoxic element [7] that highly affects almost every organ and system in the human body [9].

The ACs possess a large specific surface area and high porosity and therefore a high adsorption capacity for heavy metals [10]. The physical and chemical properties of the AC and its suitability for wastewater treatment (sorption ability) is widely attributed to the initial properties of the precursor as well as the synthesis method, and the activation conditions [11]. A proper engineering of the surface properties improves the interactions between adsorbents and adsorbates [12]. Surface modification of lignocellulosic biomass with different chemical solutions to improve the surface area and pore volume as well as functional groups, and play a decisive role in the improvement of adsorption performance and its selectivity on a certain adsorbate [13]. The chelating efficiency of AC can be enhanced by extracting soluble organic compounds of lignocellulosic waste [14]. Acid pretreatment of biomass may react with the inorganics and modify the available functional groups and the pore structure. Pretreatment of biomass with HNO_3 may produce AC with similar size pores but a large variety of surface functional groups (e.g. carbonyl, carboxyl, and nitrate groups). HCl-pretreated AC produced oxygen functional groups like phenols, ethers, and lactones [15].

* Corresponding author.
E-mail address: mnorolah@iut.ac.ir (N. Mirghaffari).

https://doi.org/10.1016/j.ijbiomac.2021.03.078
0141-8130/

Moreover, AC obtained from pretreated carbonaceous waste with alkali and alkali earth metal salts demonstrated impressive sorption of various contaminants [16,17]. Ling et al. (2017) found that magnesium oxide (MgO) embedded biochar composites showed high adsorption capacity for heavy metals due to the specific porous structure and ion exchange [12]. Yuan et al. (2018) reported that AC prepared from co-pyrolysis of biomass and magnesium chloride ($MgCl_2$) showed oxygen functional groups and lots of pores with the same size as MgO grains [18].

However, the effect of different pretreatment methods of biomass on the characteristics of prepared AC have not been comprehensively studied. Following our previous study on the preparation of high performance AC from the lignocellulosic waste of Elm tree through post thermal treatment [10], we have examined the efficiency of chemical pretreatment methods of this waste for heavy metals removal. The alkali and alkali earth metal salts (NaCl, KCl, $MgCl_2$, $CaCl_2$ and biomass ash) and leaching chemicals (water, HCl and HNO_3) were employed for pretreatment of Elm tree lignocellulosic waste as a precursor to produce AC. To our best knowledge, the synthesis of activated carbon using the presented process for Pb (II) and Cr (VI) removal was not previously reported in the literature. So, the main purpose of the current study was to investigate the effect of different biomass treatment on the physical and chemical properties of synthesized AC as well as Pb (II) and Cr (VI) removal efficiency. In addition, the changes in the physical and chemical properties of the selected samples with and without pretreatment were studied to explore adsorption mechanisms.

2. Material and methods

2.1. Materials

Elm tree sawdust was collected from green pruning waste of Isfahan University of Technology, Isfahan, Iran. Lead nitrate ($Pb(NO_3)_2$), potassium dichromate ($K_2Cr_2O_7$), potassium hydroxide (KOH), sodium chloride (NaCl), potassium chloride (KCl), calcium chloride ($CaCl_2$), magnesium chloride ($MgCl_2$), hydrochloric acid (HCl) and nitric acid (HNO_3) solutions were prepared from analytical grade materials (Merck, Germany).

2.2. Sawdust characterization

The collected sawdust was dried at 70 °C for 24 h in a conventional oven, grounded into small size (10 meshes) and characterized through its pH (ASTM D4980-89), ash content (ASTM D1102-84), extractive content (ASTM D1105-96), Lignin content (ASTM D1106-96) and cellulose content [19]. Hemicelluloses content was calculated by subtracting the sum of the above values from 100. The composition of the inorganics (alkali and alkali earth metal) was determined using a dry method [20]. One gram of Elm tree sawdust was converted to ash in a muffle furnace at 550 °C for 4 h. Then the remaining ash was digested by HNO_3 25% *v*/v (5 mL) and then the digested sample was reached to 25 mL. The amounts of Ca and Mg in the obtained solution were measured using flame atomic absorption spectroscopy (FAAS) (PerkinElmer, AAnalyst700). The concentration of Na and K was determined using a flame photometer (Flamephotometer, ELE PFP7).

Thermogravimetric analysis (TGA) was performed to understand the thermal stability from ambient temperature to 1200 °C with the heating rate of 10 °C min^{-1} under the N_2 atmosphere (Rheometric Scientific, 1998).

2.3. Activated carbon production

The reagents for pretreatment of lignocellulosic waste including the solutions of 3% *w*/w of alkali and alkaline earth metal salts (NaCl, KCl, $CaCl_2$, and $MgCl_2$) were prepared. Also, a mixture of 3% *w*/w Elm tree sawdust ash in deionized water as a cost-effective and valuable mixture for providing Na, K, Mg and Ca was provided. For deashing pretreatment of lignocellulosic waste the 3% w/w leaching solution of water, HCl, HNO_3 and aqua regia (3:1 ratio of HCl to HNO_3) were also made seperately.

The grinded Elm tree sawdust (15 g) was mixed with 150 mL of each solution together with 150 mL of deionized water and stirred for 90 min to obtain a well-mixed slurry. Then the slurry passed a filter paper (Whatman No. 42), washed with 150 mL distilled water to remove excess reagents and dried in a conventional oven at 70 °C to obtain the pretreated Elm tree sawdust as precursors for AC synthesis. Subsequently, a mixture of the pretreated biomass and KOH were prepared according to the procedure previously reported for grape seeds [21]. Briefly, 10 g of each pretreated sawdust were mixed with powdered KOH by impregnation ratio of 2:1 (KOH: sawdust). After 24 h remaining in ambient temperature, each mixture was put into a steel crucible and pyrolysis were performed using a muffle furnace for 1 h at 800 °C (heating rate of 10 °C min^{-1}) under a constant rate of 1 L min^{-1} N_2 gas to neutralize the atmosphere. Afterward, the samples were cooled to ambient temperature in N_2 atmosphere and then removed from the muffle furnace. The obtained ACs were post treated through thermal tension treatment (as explained in our previous study) [10], dried at 70 °C and then kept in capped containers.

2.4. Heavy metal adsorption experiments

2.4.1. Batch experiments

First, different Pb (II) and Cr (VI) adsorption batch experiments were conducted to assess the impact of four optimization parameters on Pb (II) and Cr (VI) adsorption by prepared ACs including adsorbent dosage (0.1 to 0.4 g L^{-1}); pH of the sample solution (2 to 5); initial metal concentrations (5 to 150 mg L^{-1}); contact time (1 to 180 min). Then, all AC samples were tested for sorption of Pb (II) and Cr (VI) in 50 mg L^{-1} of ion solution in optimized adsorption parameters. These solutions were separately prepared by adding $Pb(NO_3)_2$ or $K_2Cr_2O_7$ to distilled water and the pH was adjusted to 5.0 and 2.0, respectively. The batch adsorption experiments were conducted by mixing 0.01 g of each prepared AC with 25 mL of each solution of Pb (II) and Cr (VI) in a rotary shaker for 60 min (agitation rate: 250 rpm). Then, the suspensions were passed through a filter paper and the residual amount of Pb (II) and Cr (VI) in the supernatant were measured using FAAS (PerkinElmer, AAnalyst 700) and the Pb (II) and Cr (VI) adsorption capacities were determined according to Eq. (1) [22].

$$\text{Adsorption capacity } (q_e) = \frac{(C_i - C_e)}{M} \times V \quad (1)$$

where q_e is the concentration of adsorbate adsorbed on the adsorbent (mg g^{-1}), C_i is the initial and C_e is the equilibrium adsorbate concentrations in the solution (mg L^{-1}), V is the volume of adsorbate solution (L) and M is the dry weight of adsorbent (g).

Three kinetic models were employed to describe the adsorption process by the prepared ACs. Kinetic experiments were performed by mixing the constant AC dosage (0.4 g L^{-1}) and the Pb (II) and Cr (VI) concentration (50 mg L^{-1}) under different contact times (1, 5, 15, 30, 60, 90, 120 and 180 min) at 27 ± 2 °C. Adsorption kinetics were studied using three common kinetic models including the pseudo-first order (Eq. (2)) [23], the pseudo-second-order (Eq. (3)) and the intra-particle diffusion model (Eq. (4)) [24].

$$ln\,(q_e - q_t) = ln\,q_e - k_1 t \quad (2)$$

$$\frac{t}{q_t} = \frac{1}{k_2 q_e^2} + \frac{t}{q_e} \quad (3)$$

$$q_t = K_{id} t^{0.5} + C \quad (4)$$

where q_t and q_e (mg g^{-1}) are the amount of Pb (II) and Cr (VI) adsorbed at time t and equilibrium time, respectively. k_1, k_2 (min^{-1}) and K_{id}

($mg\ g^{-1}\ min$) are the rate constants for the pseudo-first, pseudo-second order, and intra-particle diffusion kinetic equations, respectively. C ($mg\ g^{-1}$) is an intra-particle diffusion constant that indicates the thickness of the boundary layer.

The Langmuir (Eq. (5)) [25], the Freundlich (Eq. (6)) [25] and the Temkin (Eq. (7)) [24] isothermal models were used to describe the adsorption process by the prepared ACs. Isothermal experiments were conducted by mixing a constant AC dosage (0.4 g L^{-1}) and contact time (60 min) with the different Pb (II) and Cr (VI) initial concentrations (10 to 300 mg L^{-1}) at 27 ± 2 °C.

$$\frac{C_e}{q_e} = \frac{1}{K_L q_m} + \frac{C_e}{q_m} \tag{5}$$

$$ln\, q_e = ln\, K_F + \frac{1}{n} ln\, C_e \tag{6}$$

$$q_e = \frac{RT}{b_T} ln\, K_T + \left(\frac{RT}{b_T}\right) ln\, C_e \tag{7}$$

where C_e ($mg\ L^{-1}$) is the equilibrium concentration of adsorbate in the aqueous solution, q_e and q_m ($mg\ g^{-1}$) are the equilibrium and maximum adsorption capacity of adsorbate per unit weight of adsorbent, respectively. K_L ($L\ mg^{-1}$) is the Langmuir isotherm constant which is related to the affinity of the binding sites, respectively, b_T ($g\ kJ\ mg^{-1}\ mol^{-1}$) is the Temkin isotherm constant related to the heat of adsorption. K_T ($L\ mg^{-1}$) is the equilibrium binding constant corresponding to the maximum binding energy ($L\ mg^{-1}$), T is the temperature (K), and R is the ideal gas constant (8.314 kJ $mol^{-1}\ K^{-1}$), K_F ($mg^{1-1/n}L^{1/n}g^{-1}$) and n (dimensionless) are the Freundlich constants representing the adsorption capacity and intensity, indicating the favorability of adsorption. A higher value of K_f demonstrates a higher adsorption capacity. n^{-1}, ranging between 0 and 1, is indicative of the surface heterogeneity and lower value shows a more heterogeneous surface [26]. Moreover, to determine the fitness between the experimental data and predicted adsorption capacities in each model, the average relative error (ARE) was calculated [27] (Eq. (8)).

$$ARE\ (\%) = \frac{100}{n} \sum_{i=1}^{n} \left| \frac{q_{e\ meas} - q_{e\ calc}}{q_{e\ meas}} \right| \tag{8}$$

where $q_{e\ calc}$ and $q_{e\ meas}$ are the calculated and measured adsorption capacity of adsorbate per unit weight of adsorbent at equilibrium ($mg\ g^{-1}$).

Three industrial wastewater obtained from local industries, galvanic, chemical and textile printing, were used to evaluate the Pb (II) and Cr (VI) adsorption efficiency of selected AC in a real matrix of industrial wastewater. Some characteristics of these wastewaters were determined and tabulated in Table 1. The initial Pb (II) and Cr (VI) concentration of the wastewater samples was adjusted at 10 mg L^{-1} by adding the metal solutions and the pH of the samples was fixed on 5.0 and 2.0 for Pb (II) and Cr (VI), respectively. Then the adsorption tests were carried out considering the same conditions as the synthetic solutions.

Table 1
Characteristics of the Elm tree lignocellulosic waste.

Chemical analysis	Value
pH	6.68
Ash (% wt)	4.20
Extractives (% wt)	4.21
Lignin (% wt)	31.0
Cellulose (% wt)	45.4
Hemicelluloses (% wt)	19.5

% wt: based on dry weight.

2.4.2. Column experiments

Continuous-flow adsorption experiments were performed in a Teflon column (100 mm height × 3 mm inner diameter). The column was packed with 0.05 g of AC and to avoid adsorbent loss, the top and bottom of the column were plugged with a small amount of glass wool. The Pb (II) and Cr (VI) solutions (each with a concentration of 50 mg L^{-1}) was separately pumped into the column at a constant 1.5 mL min^{-1} flow rate using a peristaltic pump (Sina Lab Equipment, SP15, Iran). In order to determine the breakthrough curve, effluent samples were taken at different times and the amount of Pb (II) and Cr (VI) in the samples were measured until adsorbent saturation with the adsorbate and no more adsorption took place in the bed. When this has occurred the concentration of the adsorbate in the effluent reached to the feed value (50 mg L^{-1}).

2.5. Adsorbent characterization

The surface morphology and elemental mapping of the samples were detected using scanning electron microscopy (SEM, Philips XI30 microscope at 30 kV voltage), combined with energy-dispersive X-ray spectroscopy (EDX) (Seron AIS 2300) [28]. The pellet of the samples mixed with KBr were prepared and analyzed using the Fourier transform infrared spectroscopy (FTIR) (Bruker, Tensor27) in the range of 400–4000 cm^{-1} to determine the surface chemical characteristics of the obtained ACs [29].

The textural characteristics of the samples were investigated using N_2 adsorption/desorption at 77 K. After degassing the AC samples at 250 °C under vacuum for 2 h, the N_2 adsorption isotherm was used to evaluate the specific surface areas using Brunauer, Emmett, and Teller (BET) equation at the relative pressure (0.001–0.3 bar). The total pore volumes were calculated from the amount of N_2 adsorbed at $P\ P_0^{-1} = 0.995$ [30]. The distribution of micropores was determined through micropore analysis method (Micropore Plots (MP) method) [30,31]. The volume and distribution of mesopore were obtained from desorption isotherms using the Barrett–Joyner–Halenda (BJH) method [32].

2.6. Desorption experiments

HCl and $CaCl_2$ solutions (0.5 M) were used as eluents to desorbe Pb (II) and Cr (VI) from saturated adsorbents. About 0.01 g of $MgCl_2$ -pretreated and non-pretreated AC was dried at 70 °C after the Pb (II) adsorption and then soaked in 50 mL of HCl solution during stirring at 250 rpm. A similar procedure was conducted to desorbe Cr (VI) from HCl pretreated and non-pretreated AC with $CaCl_2$ solution. At the final step, the concentrations of the desorbed Pb (II) and Cr (VI) in the solutions were measured and the desorption efficiency (%) was calculated as follows [21]:

$$D\% = \left(\frac{q_{e\ desorption}}{q_{e\ sorption}}\right) \times 100 \tag{9}$$

where D is the metal desorption efficiency (%), $q_{e,\ sorption}$ and $q_{e,\ desorption}$ are the metal sorption and desorption capacity ($mg\ g^{-1}$), respectively. The metal desorption capacity was calculated using the following equation:

$$q_{e\ desorption} = \frac{V\ C_f}{M} \tag{10}$$

where q_e is the amount of metal desorbed from loaded adsorbent ($mg\ g^{-1}$), C_f is the metal concentration in the eluent solution ($mg\ L^{-1}$), V is the eluent solution volume (L), and M is the adsorbent weight (g).

2.7. Statistical analysis

SPSS computer software (version 21) was used to analyze the experimental data. The one-way analysis of variance (ANOVA) was conducted

to determine the significant effects of different pretreatments on Pb (II) and Cr (VI) adsorption capacity of obtained ACs.

3. Results and discussion

3.1. Lignocellulosic waste characterization

The characteristics of Elm tree sawdust including the content of extractives, lignin, cellulose, and hemicellulose are tabulated in Table 1. Lignocellulosic waste mainly consists of lignin, cellulose, and hemicellulose. Based on literature, lignin is a major component for the production of ACs [33]. The amount of lignin in the Elm tree sawdust was 30.99%, which is suitable for AC production. Moreover, its low content of ash is a suitable factor to achieve a high yield of AC production [34]. Meanwhile, results from the TGA experiment of Elm tree sawdust pointed out three thermal degradation stages which can be attributed to the moisture elimination (up to 150 °C), decomposition of hemicelluloses and celluloses (180–400 °C) and the decomposition of high stability component (400–550 °C). The decomposition of lignin, which is a major fraction, occurred slowly and continuously from 200 °C to 900 °C (Fig. 1) [10].

The amount of alkali and alkaline earth metals of the ELM tree sawdust ash were 11, 74, 540 and 25 mg g^{-1} for Na, K, Ca and Mg, respectively. Treating the sawdust using 1.0 g of sawdust ash provide 650 mg of the total alkali and alkaline earth elements. This may be played the role of chemical salts in the precursor pretreatment for activated carbon preparation.

3.2. Batch adsorption experiments

The results of the parameters affecting the adsorption process revealed that pH = 5, sorbent dosage = 0.4 g L^{-1}, initial concentration = 50 mg L^{-1} and contact time = 60 min for Pb were the optimum factors, whereas the relevant amounts for Cr were 2, 0.4 g L^{-1}, 50 mg L^{-1} and 60 min, respectively (Fig. S1). To evaluate the effectiveness of the precursor pretreatment, the produced ACs were used in Pb (II) and Cr (VI) adsorption experiments (Fig. 2). It is obvious that the precursor pretreatment with alkali and alkaline earth metals could increase the Pb (II) adsorption capacity by pretreated ACs but this pretreatment decreased the Cr (VI) adsorption capacity ($P < 0.01$). On the other hand, leaching the precursor with water, HNO_3, HCl and aqua regia were able to significantly increase the Cr (VI) adsorption capacity of the AC but decreased the Pb (II) adsorption capacity ($P < 0.01$).

Biomass leaching and biomass acid washing with HCl and HNO_3, and aquafortis, lead to the removal of elements as well as extractable and hemicellulose contents from biomass [35]. Biomass leaching removes

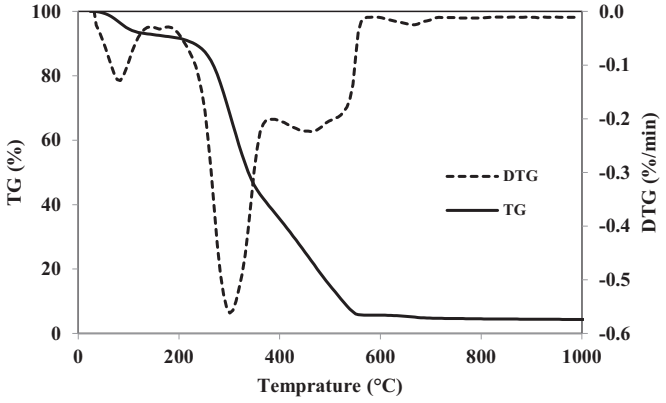

Fig. 1. Thermogravimetric analysis (TGA) of Elm tree waste.

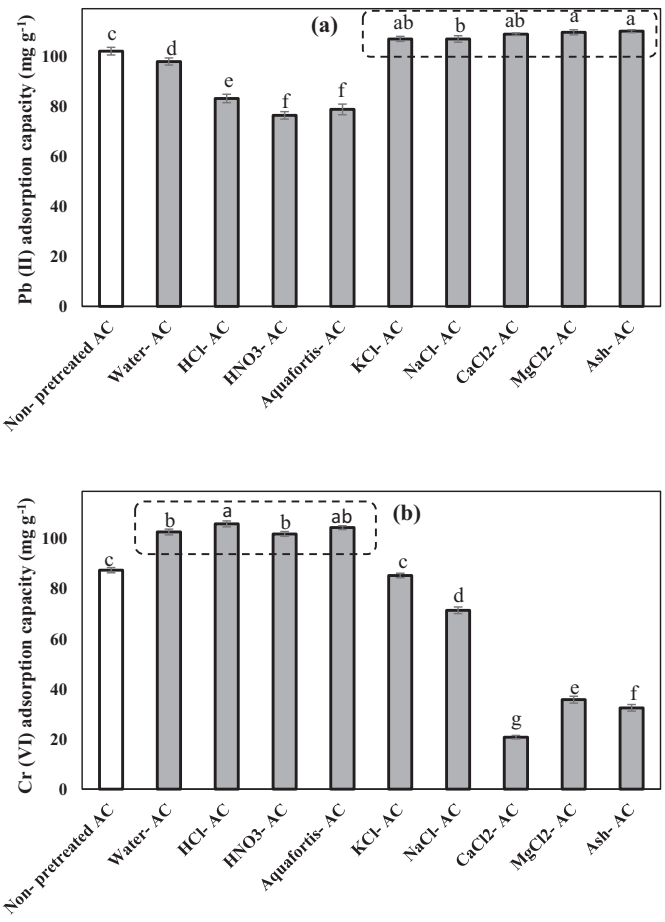

Fig. 2. The effect of precourse pretreatment on (a) Pb (II) and (b) Cr (VI) adsorption capacity of ACs prepared from Elm tree sawdust (adsorbent dosage, 0.4 g L^{-1}; Pb (II) and Cr (VI) solution concentration, 50 mg L^{-1} in pH, 5 and 2, respectively; contact time, 60 min; agitation speed, 250 rpm). Same letters show an insignificant difference by the Duncan test ($P > 0.05$).

alkali metals such as Na and K from biomass. Moreover, acid washing can also remove other alkali metals such as Mg, Ca and Al from biomass [36]. As evident from literature, single acid, particularly HCl or a blend of acids, like HCl and HNO_3 play a decisive role to remove ash [15]. It should be pointed out that contrary to HNO_3, HCl is not an oxidant and therefore it can be safely utilized in the deashing process without destroying the biomass structure [37]. The presence of alkali metals (Na and K) and to a lesser extent alkaline earth metals (Mg and Ca) in biomass acts as a catalyst in the biomass thermal decomposition process and increases the rate of char production [38]. In various studies, the effect of using inorganic salts such as NaCl, KCl, $MgCl_2$, and $CaCl_2$ on the fast pyrolysis process has been studied and showed that the presence of alkali and alkaline earth metals increased the rate of char production, significantly [39].

3.3. Adsorption modeling

3.3.1. Adsorption kinetic

Adsorption kinetics were studied using three common kinetic models including the pseudo-first, pseudo-second-order and intra-particle diffusion model. The adsorption data of Pb (II) and Cr (VI) were well fitted to the pseudo-second order kinetic model with a linear regression correlation coefficients (R^2) more than 0.99 for all obtained ACs (Table 2). The surface chemisorption involves electron change and physicochemical interactions between the adsorbate and the adsorbent are the rate limiting step in this model [40].

Table 2
Derived parameters in the kinetic models for adsorption of Pb (II) and Cr (VI) by pretreated ACs from Elm tree sawdust.

Metal	Adsorbent	Pseudo-first-order			Pseudo-second-order		
		q_e	$K_1 \times 10^2$	R^2	q_e	$K_2 \times 10^2$	R^2
Pb (II)	Non-pretreated AC	22.0	1.6	0.40	133	0.50	0.99
	NaCl- pretreated AC	15.1	1.4	0.58	127	0.90	0.99
	KCl- pretreated AC	19.8	1.6	0.75	127	6.1	0.99
	$CaCl_2$- pretreated AC	11.8	2.7	0.56	145	0.60	0.99
	$MgCl_2$- pretreated AC	3.70	1.8	0.73	148	2.9	1.0
	Ash- pretreated AC	3.30	1.7	0.75	145	3.4	1.0
Cr (VI)	Non-pretreated AC	11.3	1.7	0.73	97.0	0.70	1.0
	Water- pretreated AC	33.6	0.90	0.72	103	0.30	0.99
	HNO_3- pretreated AC	33.6	0.90	0.82	105	0.30	0.99
	Aquafortis- pretreated AC	36.4	1.0	0.81	106	0.20	0.99
	HCl- pretreated AC	28.7	1.0	0.79	109	0.30	0.99

Table 3
Slopes (K_{id}) from intraparticle diffusion equation for Pb (II) and Cr (VI) adsorption with obtained pretreated ACs from Elm tree sawdust.

Metal	Adsorbent	K_{id} (mg g^{-1} min^{-1})			
		K_{id1}	R^2	K_{id2}	R^2
Pb (II)	Non-pretreated AC	6.92	0.96	0.090	0.99
	NaCl- pretreated AC	6.01	0.97	0.090	0.99
	KCl- pretreated AC	6.10	0.98	0.090	0.99
	$CaCl_2$- pretreated AC	12.2	0.99	0.020	0.99
	$MgCl_2$- pretreated AC	0.470	0.83		
	Ash- pretreated AC	0.410	0.82		
Cr (VI)	Non-pretreated AC	1.73	0.99	0.50	0.94
	Water- pretreated AC	1.36	0.93	0.43	0.96
	HNO_3- pretreated AC	1.36	0.93	0.40	0.99
	Aquafortis- pretreated AC	1.47	0.97	0.40	0.99
	HCl- pretreated AC	1.65	0.99	0.22	0.99

To further realizing the diffusion mechanism and the rate controlling steps for the Pb (II) and Cr (VI) adsorption, the intra-particle diffusion model was also investigated (Fig. 3). According to this model, when the plot of q_t vs $t^{1/2}$ is a straight line, it indicates that the intraparticle diffusion is the only rate limiting step of the adsorption process [41]. While the data present a multi-linearity, the sorption process is controlled by two or more steps which means the intra-particle rate diffusion is not the only rate limiting step in the adsorption process [42]. Both the film diffusion and the intra-particle diffusion might control the adsorption of pollutants on the porous adsorbent's surface [43]. At first, the external mass transfer was done with higher rate constants by macropores and mesopores followed by intraparticle diffusion with lower rate constant by micropores [44].

The plot Cr (VI) q_t vs $t^{1/2}$ exhibited two straight lines for non-pretreated and pretreated ACs due to the different mass transfer rate in the wide range of contact time (Fig. 3c) [10]. The intraparticle diffusion constants (K_{id}) of each stage can be calculated using Eq. (9). K_{id1}, K_{id2} and the correlation coefficient (R^2) are listed in Table 3. It is obvious that the adsorption rate of the first stage is much higher than the second stage due to the significant difference in the slopes. In the first stage, the Cr (VI) ions adsorbed to external macro and mesopores. Therefore, the adsorption rate for this section was very high. After saturation of macropores, Cr (VI) ions penetrated to the internal surface of particle pores and adsorbed by the micropores. Diffusion of Cr (VI) ions to the micropore surfaces leads to increasing the diffusion resistance and thus decreasing the diffusion rate [41]. In this sense, in Pb (II) adsorption process, two straight lines were expected for non- pretreated, NaCl, KCl and $CaCl_2$ pretreated ACs (Fig. 3a) while three ACs ($MgCl_2$ and ash pretreated ACs) presented a single straight line (Fig. 3b). It indicates that the solely controlling step for Pb (II) sorption on these ACs is intraparticle diffusion, which can be attributed to maximum access to micropores through the presence of a large number of mesopores created.

3.3.2. Adsorption isotherm

To design the adsorption process, Pb (II) and Cr (VI) experimental data of selected ACs were fitted to the Langmuir, Freundlich and Temkin isotherm models.

The results revealed that the Cr (VI) adsorption data of all obtained ACs showed more compliance with the Temkin isotherm with a higher R^2 and lower average relative error comparing to the other models

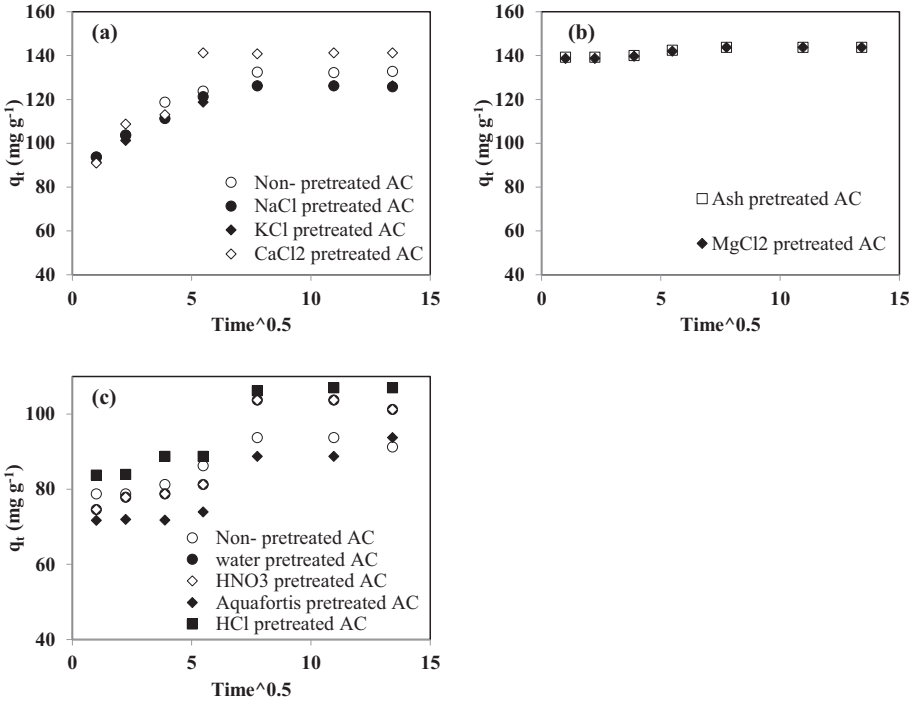

Fig. 3. Intra-particle diffusion plots for Pb (II) (a, b) and Cr (VI) (c) adsorption on the pretreated ACs from Elm tree sawdust.

Table 4
Parameters of adsorption isotherms for Pb (II) and Cr (VI) by pretreated ACs produced from Elm tree lignocellulosic waste.

Metal	Adsorbent	Langmuir				Freundlich				Temkin			
		q_m (mg g^{-1})	K_L (L mg^{-1})	R^2	ARE (%)	k_f ($mg^{1-1/n}L^{1/n}$ g^{-1})	n	R^2	ARE (%)	b_T (g kJ mg^{-1} mol^{-1})	K_T (L mg^{-1})	R^2	ARE (%)
Pb (II)	Non-pretreated AC	233	0.42	0.98	40.7	82.3	3.6	0.83	24.5	91.3	47.9	0.95	16.7
	NaCl-AC	313	0.061	0.98	44.5	68.3	3.8	0.94	15.2	80.2	18.7	0.95	14.1
	KCl-AC	286	0.065	0.97	42.1	68.1	4.0	0.93	18.6	86.6	23.1	0.96	11.2
	$CaCl_2$-AC	501	0.18	0.99	32.8	101	2.9	0.84	34.2	39.9	14.3	0.85	35.5
	$MgCl_2$- AC	1430	0.14	0.99	9.17	152	1.5	0.97	17.5	12.4	4.61	0.88	171
	Ash-AC	1250	0.086	0.99	12.5	98.5	1.5	0.95	22.7	13.2	2.38	0.90	138
Cr (VI)	Non-pretreated AC	114	0.18	0.98	12.3	19.4	2.0	0.87	20.2	96.6	1.61	0.93	11.3
	Water-AC	179	0.14	0.97	12.0	22.8	1.7	0.88	22.1	71.3	1.53	0.96	11.5
	HNO_3-AC	143	0.17	0.97	13.4	21.7	1.8	0.85	23.4	76.4	1.56	0.93	13.3
	Aquafortis-AC	185	0.13	0.98	9.61	22.8	1.6	0.91	18.2	65.1	1.39	0.99	6.32
	HCl-AC	190	0.15	0.97	8.60	25.0	1.6	0.92	19.0	60.1	1.57	0.98	5.41

ARE: Average relative error.

(Table 4). Also, the isotherms of Pb (II) adsorption on non- pretreated AC and NaCl and KCl pretreated ACs were well fitted with the Temkin model. In this model, due to the interaction of the adsorbent and adsorbate, the decrease in the heat of adsorption of adsorbate molecules on the surface layer decrease linearly (not logarithmically) with the increase in the extent of adsorption [45]. A uniform distribution of binding energy (up to some maximum binding energy) is a characteristic of adsorption [46]. In contrast, it's evident that after pretreatment of biomass with alkali and alkaline earth metal, the Langmuir isotherm was better fitted for Pb (II) adsorption on $CaCl_2$, ash, and $MgCl_2$ pretreated ACs. The compliance of the adsorption with the Langmuir isotherm model illustrated the chemisorption with a monolayer and homogenous sorption [40]. The obtained ACs demonstrated significantly higher Pb (II) and Cr (VI) maximum adsorption capacity than the non-pretreated one. The Pb (II) maximum adsorption capacity obtained with ash, and $MgCl_2$ pretreated ACs were 1250 and 1430 mg g^{-1}, respectively which were higher than those published in the literature (Table 5). It confirms the effectiveness of Mg pretreatment of biomass on the AC Pb (II) adsorption capacity. Besides, the maximum Cr (VI) adsorption capacities were observed for leached pretreated ACs which were significantly higher than that of non-pretreated ACs. Aqua regia and HCl pretreated ACs showed the highest adsorption capacity (185 and 190 mg g^{-1}, respectively) indicated the usefulness of biomass leaching in increasing Cr (VI) adsorption capacity. Therefore, according to the obtained results, all further experiments and characterizations were conducted using $MgCl_2$ and HCl pretreated ACs which demonstrated the highest Pb (II) and Cr (VI) adsorption capacity, respectively.

3.4. Activated carbon characterization

3.4.1. SEM and EDX analysis

The SEM image and EDX spectrum of non- treated AC shows a porous morphology (due to the derivative compounds evaporation of activating agent [47]) and C, O, Mg, Al, Si and Ca as the main components (Fig. 4) [10]. The success of the $MgCl_2$ biomass pretreatment is confirmed by intensive Mg and O peaks in the EDX spectrum which demonstrated the formation of MgO from $MgCl_2$ during pyrolysis at high temperature. Other elements, such as Al and Ca were replaced by Mg and released during $MgCl_2$ treatment. The SEM image of $MgCl_2$- pretreated AC shows a carbon sheet with many MgO nanoparticles.

As expected, the same trend was not observed for HCl- pretreated AC. The EDX elemental analysis showed a drastic increase in C content and reduction in Mg, Si and Ca content. Comparing the number and the size of the cavities within the 10-μm range exhibited the development of a larger number of micropores in SEM micrographs of HCl- pretreated AC.

3.4.2. N_2 adsorption/desorption isotherms

The nitrogen adsorption/desorption isotherms and pore size distribution of prepared ACs were conducted to explore the effect of biomass pretreatment on the pore forming process during pyrolysis. Fig. 5

Table 5
The Pb (II) and Cr (VI) maximum adsorption capacities of various lignocellulosic-based activated carbons reported in the literature.

Adsorbed metal	Raw material	Activating agent	BET (m^2 g^{-1})	pH solution	q_m (mg g^{-1})	Reference
Pb (II)	Palm shell	–	957	3.0	82.0	[56]
	Branches of walnut wood	HNO_3	32.0	7.0	58.8	[57]
	Polygonum orientale Linn	H_3PO_4	1390	5.0	98.4	[58]
	Water hyacinth stems	H_3PO_4	381	5.0	175	[26]
	Lemna minor	H_3PO_4	532	6.0	171	[59]
	Coconut shell	–	999	5.6	76.6	[60]
	Hazelnut husks	$ZnCl_2$	1090	5.7	13.1	[61]
	Mangifera indica seed shell	H_2SO_4	94.1	3.0	122	[62]
	Sugarcane bagasse	H_3PO_4	321	4.0	8.58	[63]
	Coffee residue	$ZnCl_2$	891	5.8	63.0	[64]
	$MgCl_2$ pretreated Elm tree sawdust	KOH	585	5.0	1430	Present study
Cr (VI)	Groundnut husk	H_2SO_4	–	3.0	7.00	[65]
	Peanut shell	KOH	95.5	2.0	16.3	[66]
	Mango Kernel	H_3PO_4	491	2.0	7.80	[67]
	Rubberwood sawdust	H_3PO_4	1670	2.0	44.1	[68]
	Eucalyptus sawdust	KOH	18.7	2.0	45.9	[69]
	Coconut tree sawdust	H_2SO_4	486	3.0	3.46	[70]
	longan seed	NaOH	1510	3.0	169	[71]
	Thermo-compressed Firwood	KOH	1250	3.0	181	[72]
	Tamarind hull	H_3PO_4	431	2.0	85.9	[73]
	Bael fruit shell	H_3PO_4	–	3.0	17.3	[74]
	HCl pretreated Elm tree sawdust	KOH	1280	2.0	190	Present study

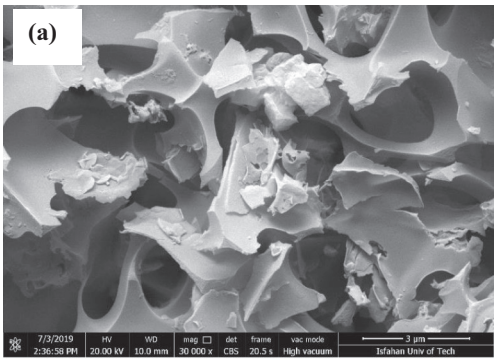

Element	Weight %	Atomic %
C	53.1	68.2
O	21.7	21.0
Mg	2.56	1.63
Al	1.06	0.610
Si	1.78	0.980
Ca	19.8	7.62

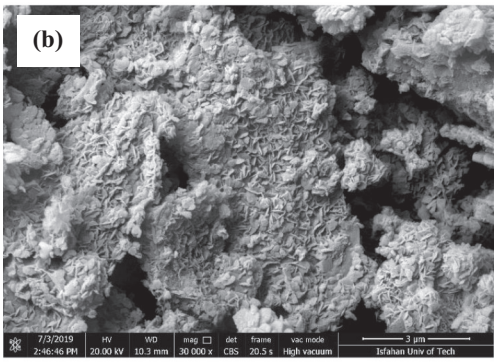

Element	Weight %	Atomic %
C	20	30
O	39	43
Mg	26	19
Al	1.0	1.0
Si	6.0	4.0
Ca	8.0	3.0

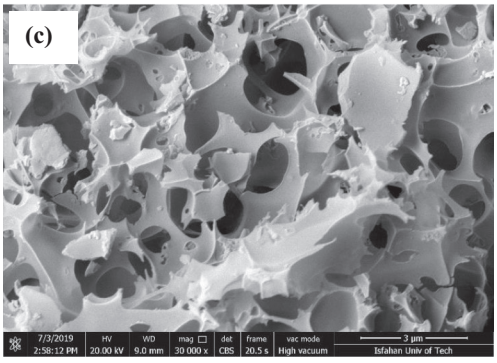

Element	Weight %	Atomic %
C	79	84
O	16	13
Mg	2.0	1.0
Al	1.0	1.0
Si	2.0	1.0

Fig. 4. SEM micrographs (×30,000) and EDX analysis of (a) Non- pretreated AC, (b) $MgCl_2$- pretreated AC and (c) HCl- pretreated ACs produced from Elm tree sawdust.

demonstrated a hybrid of type-I (at very low relative pressures) and type-IV (at moderate and high pressures) N_2 isotherm with H4 hysteresis loop indicating slit shaped pores for non- pretreated AC [10]. The isotherm of HCl- pretreated AC exhibited again a type-I (at very low relative pressures) and type-IV (at moderate and high pressures) N_2 isotherm with H4 hysteresis loop but with more N_2 adsorption capacity which demonstrated greater BET surface area and microporosity. The steep N_2 adsorption at low relative pressure (~0.1 P P_0^{-1}) in type-I isotherms corresponded to the development of micropores in materials. Type-IV isotherms with small hysteresis at moderate and high pressures

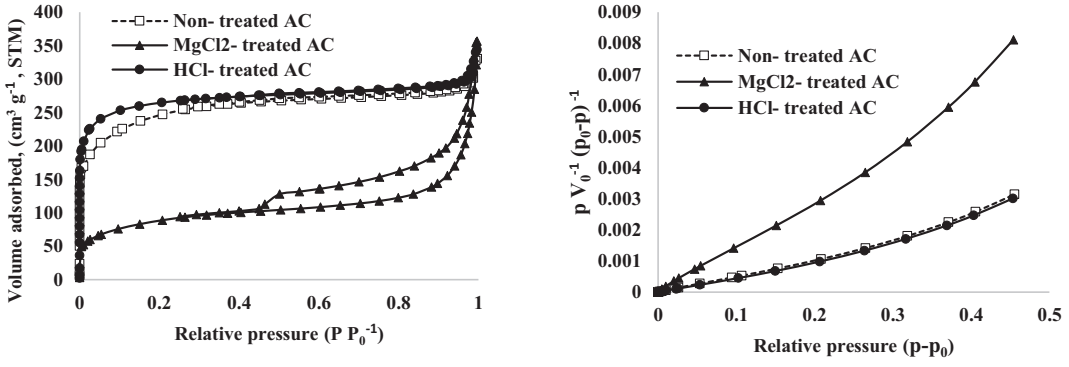

Fig. 5. N_2 adsorption/desorption isotherms of the prepared activated carbons from Elm tree sawdust.

Table 6
Textural properties of non- pretreated, $MgCl_2$ and HCl pretreated activated carbons prepared from the lignocellulosic waste of Elm tree.

Sample	S_{BET} ($m^2\ g^{-1}$)	V_{total} ($cm^3\ g^{-1}$)	V_{mic} ($cm^3\ g^{-1}$)	V_{mes} ($cm^3\ g^{-1}$)	D_p (nm)
Non-pretreated AC	1080	0.499	0.423	0.0761	1.76
HCl pretreated AC	1280	0.499	0.443	0.0570	1.61
$MgCl_2$ pretreated AC	585	0.476	0.129	0.347	4.87

indicate the presence of some mesopores in the adsorbent [48]. $MgCl_2$ pretreated AC exhibited type-IV N_2 isotherm with an obvious H_3 hysteresis loop at 0.4–0.9 P P_0^{-1} indicated the development of abundant mesopores in AC [18]. The detailed results of the pore structures including the specific surface area (S_{BET}), mesopore volume (Vmes), total pore volume (Vtotal) and average pore diameter (Dp) are found in Table 6. The results revealed that the HCl pretreatment of biomass developed the porous structure, resulting in an increased BET surface area and a decreased average pore diameter compared with the non- pretreated sample. The BET surface area of HCl- pretreated AC was 1280 $m^2\ g^{-1}$ which is higher than the non- pretreated AC (1085 $m^2\ g^{-1}$). As leaching of biomass prior to the pyrolysis process can dissolve impurities, it may produce more carbon- free active sites, which could be developed into pores [49]. Removal of catalytic metallic species during acid pretreatment may cause reduced reactivity of the char, thus allowing better diffusion of the activating agent into the carbon matrix and development of porosity [50]. Das et al. (2004) concluded that the surface area increment occurs due to the elimination of metal cationic compounds during biomass leaching and opening of metal cation blocked silica pores [35]. In addition, an increase in micropore volume and a decrease in mesopore volume were observed for HCl- pretreated AC in comparison with non- treated AC which can be attributed to the removal of deterioration of narrow mesopores. Elimination of Si after acid pretreatment reduced the formation of SiO_2 accumulated mainly in the outer layers, preventing the development of pore structure. Acid leaching of biomass not only removed the Si rich protective layer but also separated the three main components of biomass (cellulose, lignin, and hemicelluloses), promoting the porous structure [51]. Furthermore, HCl pretreatment of lignocellulosic waste dissolved the main metallic impurities like Mg, Ca, Na, K, Fe, and P which were distributed all over the biomass [15] and thus improved the formation of the porous structure.

The $MgCl_2$ pretreated AC showed a much greater fraction of mesoporosity comparing to the microporous nature of non- pretreated and HCl- pretreated ACs (Table 6). This statement is confirmed by the type-IV N_2 adsorption/desorption isotherm indicating the development of considerable mesopores. The rapid increase in N_2 uptake at ~0.1 P P_0^{-1} and 0.4–0.9 P P_0^{-1} attributed to the existence of micropore and abundance of mesopores [18]. Furthermore, the comparison of average pore diameter approved the considerable effect of $MgCl_2$ biomass pretreatment on mesopore development. The average pore diameter of $MgCl_2$ pretreated AC was 4.87 nm which was much greater than both non- pretreated and HCl- pretreated ACs. It should be pointed out that as the average pore diameter increased, the specific surface area of $MgCl_2$- pretreated AC decreased [52]. The utilization of magnesium salt during the preparation of AC can act as a promising pore-forming agent [53]. The strong capability of $MgCl_2$ in dehydration of carbohydrate polymers like lignocellulosic biomass at high temperatures prevents heavy tar formation that may clog the pores during pyrolysis and thus produce porous structure in carbon matrix [18]. Moreover, the $MgCl_2$ is dehydrated and decomposed to MgO grain under the pyrolysis conditions which is thought to act as an in-situ template to create a porous structure in the pyrolysis process (Eqs. (11)–(13)). The biomass formed a carbon layer on MgO that prevents the growth of MgO grains. After the dissolution of MgO, the porous structure is formed in produced char [54]. Similar pathways have also been reported during the pyrolysis of magnesium acetate ($Mg(CH_3COO)_2$) and magnesium citrate ($Mg_3(C_6H_5O_7)_2$) preloaded the carbon precursors [55,56].

$$MgCl_2.6H_2O \rightarrow MgCl_2.2H_2O + 4H_2O \uparrow \quad (11)$$

$$MgCl_2.2H_2O \rightarrow Mg(OH)Cl + H_2O \uparrow + HCl \uparrow \quad (12)$$

$$Mg(OH)Cl \rightarrow MgO + HCl \uparrow \quad (13)$$

The observed results are supported by the pore size distribution calculated using the BJH theory and MP analysis (Fig. 6). The predominant pore sizes of non-treated and HCl- pretreated ACs (peak in BJH plot (Fig. 6b)) were in the micropore region (less than 1 nm) which were confirmed through MP analysis (Fig. 6a). Meanwhile, the $MgCl_2$ pretreatment showed drastic effects on the pore structure of prepared AC. $MgCl_2$ pretreated AC has a wider pore size distribution in mesopore region than non-pretreated and HCl pretreated ACs. As shown in Fig. 6a the MP distribution plot of the $MgCl_2$- treated ACs showed no peak in the micropore region. The presence of $MgCl_2$ contributed in the widening of micropores leading to the formation of a porous structure rich in mesopores and some micropores.

3.4.3. FTIR analysis

The adsorption behavior of prepared ACs depends not only on the porous structure of AC but also on the presence of the functional groups at the AC surface with different chemical reactivity [29]. Oxygen, nitrogen, halogen, and hydrogen are the main types of atoms which affect the surface properties of ACs through bonding to the edge of the carbon layers and formation of functional groups [57]. The FTIR spectra of the non- treated HCl -pretreated and $MgCl_2$ -pretreated ACs are depicted in Fig. 7 which were similar for most of the wavelengths as reported before [10]. The wide peak in the range of 3100–3600 cm^{-1} indicated the presence of phenolic, alcoholic and carboxylic acid -OH groups in

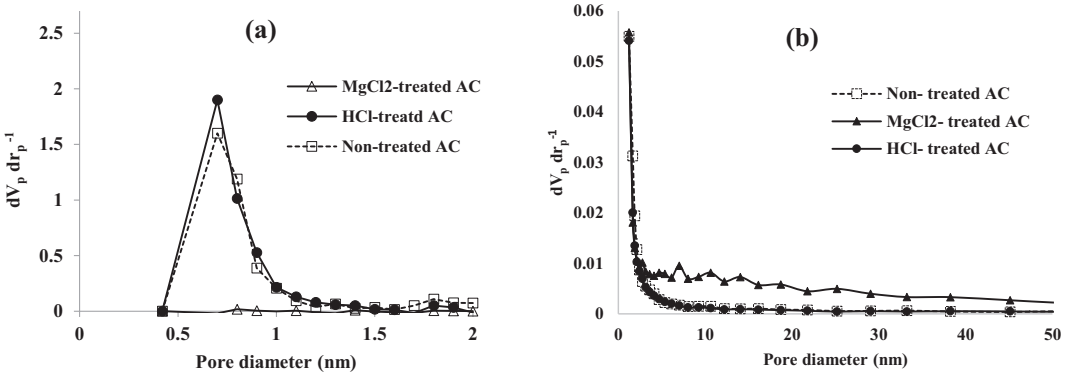

Fig. 6. (a) MP pores size distribution (<1 nm) and (b) BJH pores size distribution (>1 nm) of prepared activated carbons from Elm tree sawdust.

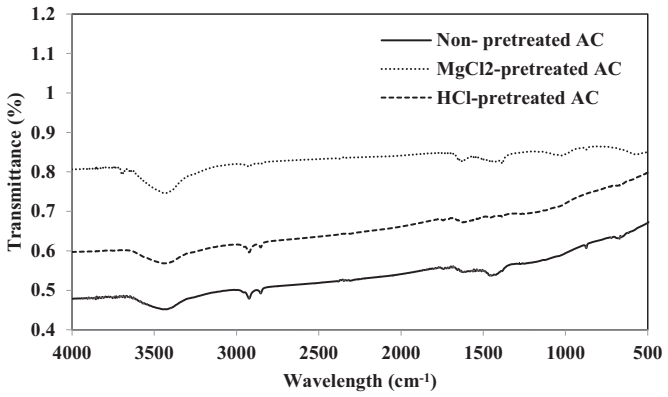

Fig. 7. FTIR spectra of prepared activated carbons from the lignocellulosic waste of Elm tree.

prepared ACs [30,58] which intensified with $MgCl_2$ pretreatment. It is noteworthy to mention that the -OH functional group play an important role in Pb ions adsorption by lignocellulose materials [40]. Similar observations were made by Yu et al. (2016) while studying the synthesis of MgO doped biochar from agricultural residues [52]. The peak between 2800 and 2900 cm^{-1} belongs to -CH group [30,59] methyl or methylene [40]. Higher intensity of this peak in non- pretreated AC comparing to the $MgCl_2$ pretreated AC may be attributed to Mg doped in such region. The peak located at 1600 cm^{-1} indicates the C═C band of the aromatic rings which may form through the decomposition of the C—H bond at high carbonization temperatures. The conjugation of aromatic rings with C═O groups may also form carbonyl-containing groups [60]. The peak at 600–900 cm^{-1} ascribed to Si—O stretching and out of plate bending of C—H [15] which disappeared in the spectra of HCl pretreated AC, indicating that the deashing of the biomass promoted Si—O and C—H breakage of the prepared AC.

3.5. Adsorption experiments using industrial wastewater

The suitability of the synthesized ACs for the removal of Pb (II) and Cr (VI) from real wastewaters were evaluated by the adsorption experiments using the galvanic industry, the chemical industry, and the textile printing company wastewaters. The results (Table 7) revealed that the adsorption efficiency of both non- pretreated AC and $MgCl_2$ pretreated AC for Pb (II) removal in 10 mg L^{-1} Pb (II) of these wastewaters were very high (more than 95%). Meanwhile, the Cr (VI) adsorption capacities with HCl pretreated AC were higher than that of non-pretreated AC. These results confirm the high efficiency of prepared AC for Pb (II) and Cr (VI) removal in industrial wastewaters.

3.6. Column adsorption experiments

The breakthrough curve for Pb (II) and Cr (VI) at 1.5 mL min^{-1} constant flow rate and 50 mg L^{-1} influent concentration of each heavy metal solution is depicted in Fig. 8. The results showed that the breakthrough and exhaustion time increased significantly for pretreated AC comparing to that of non-pretreated. This indicates the presence of a more available active sites on the pretreated ACs for heavy metal adsorption. As can be seen in Fig. 8 (a), in Pb (II) removal column experiment, for the first 250 min, the effluent from the bottom of the $MgCl_2$ pre-treated activated carbon filled bed was almost free of Pb (II) ions. In this column, more than 50% of Pb (II) could be removed after 410 min and the adsorbent exhaustion happened at approximately 1260 min after the beginning of the process. However, the non-pretreated AC exhaustion time occurred at approximately 370 min. The HCl pre-treated AC packed column was performing at maximum efficiency during the first 100 min and the removal efficiency decreased to 50% of its capacity after 150 min while in the non-pretreated AC column 50% capacity was reached after around 70 min (Fig. 8 (b)). These results showed that treatment of biomass prior to the carbonization process was an effective method to increase the exhaustion time of continuous adsorption columns due to more available binding sites for adsorption.

3.7. Desorption experiment

Desorption experiments not only can regenerate the adsorbents but also make it possible to recover the valuable adsorbed components [61]. The results of Pb (II) and Cr (VI) desorption using HCl and NaOH solutions for non- pretreated and selected pretreated ACs are listed in Table 8. The results indicated that more than 91% and 99% of the adsorbed Pb (II) could be desorbed from the non-pretreated and $MgCl_2$ pretreated ACs during 1 h, respectively. More than 60% and 56% of the adsorbed Cr (VI) were desorbed from the non-pretreated and HCl pretreated ACs after 15 h, respectively. Cr (VI) desorption experimental results point out that for desorption of Cr (VI), it should remain 15 h in contact with the NaOH solution. The stronger ability of the adsorption leads to the weaker ability of the desorption [62]. Also, this indicated that some Cr (VI) adsorption sites on the surface of the AC might be irreversible sites [61]. Furthermore, as the prepared ACs are microporous, the desorption of Cr (VI) from micropores is more difficult than that from mesopores [63].

3.8. Adsorption mechanism

The surface functional groups, porous structure, and pore size are some of AC's characteristics that play a determinant role in exploring the adsorption mechanisms [11]. As evident from literature, the Pb (II) adsorption is not only attributed to the mesoporous structure of AC but also to the increment of functional groups and the abundance of cations on the AC's surface. These statements revealed that both physical adsorption and ion exchange interaction can involve in Pb (II) adsorption from aqueous solutions [64]. The mesopore fraction of AC has a considerable effect on Pb (II) adsorption due to its wide pore size distribution, the large pore volume and also its unsaturated carbon atoms and strong reactivity. Mesopores not only accelerate the diffusion of Pb (II) ions into micropores but also increase the Pb (II) adsorption capacity through equilibrium coverage increment of the micropore surface. The high volume of mesopores aid to shorten the path length of Pb (II) to the interior micropores and hence reduce the probability of pore blockage [65]. In addition to the predominant presence of mesopores on the surface of $MgCl_2$ pretreated AC (Fig. 6 and Table 7), another main

Table 7
Adsorption capacities of Pb (II) and Cr (VI) in industrial wastewater, using selected pretreated activated carbon and non-pretreated AC as reference. (biomass dosage, 0.4 g L^{-1}; Pb (II) and Cr (VI) solution concentration, 10 mg L^{-1} in pH of 5.0 and 2.0, respectively; contact time, 60 min; agitation speed, 250 rpm), (mean ± SD, $n = 3$).

Removal efficiency (%)				
	Activated carbon	Galvanic industry wastewater	Chemical industry wastewater	Textile printing company wastewater
Pb (II)	Non-pretreated AC	98.7 ± 2.14	96.9 ± 1.82	97.7 ± 2.18
	$MgCl_2$-AC	99.2 ± 1.98	97.9 ± 2.23	98.5 ± 1.64
Cr (VI)	Non-pretreated AC	67.5 ± 2.65	63.4 ± 1.54	63.7 ± 1.81
	HCl-AC	81.0 ± 2.35	75.0 ± 1.44	72.0 ± 1.89

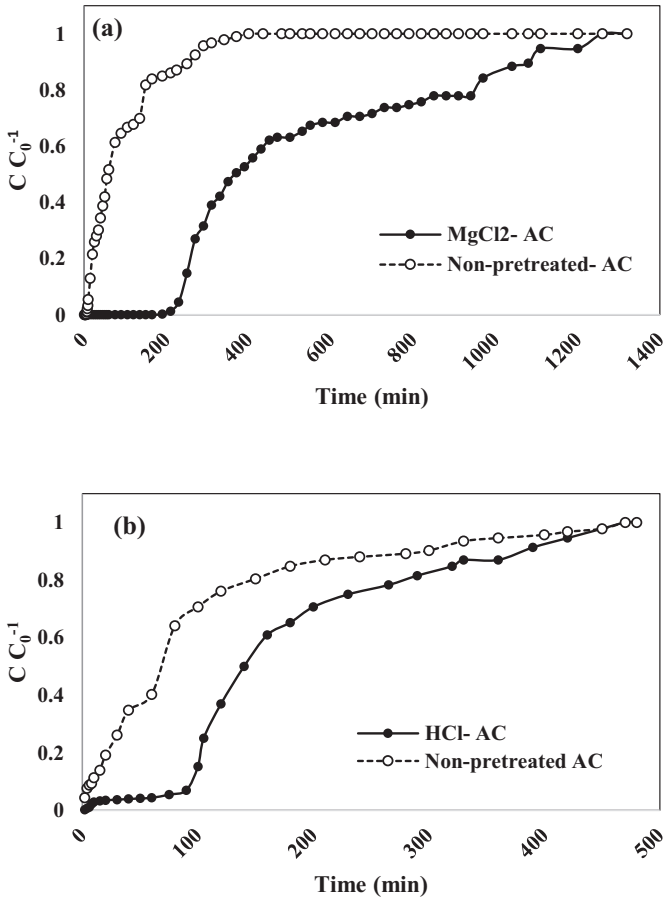

Fig. 8. The breakthrough curve of (a) Pb (II) and (b) Cr (VI) adsorption by selected pretreated and non-pretreated activated carbon.

mechanism of the Pb (II) adsorption is the ion exchange between Pb (II) and Mg. During the adsorption process, the interaction between Pb (II) and Mg may lead to the release of Mg from the $MgCl_2$ pretreated AC to the solution and adsorb Pb (II) from the solution (Fig. 5b). Therefore, the higher amount of Mg on AC's surface, the higher ion exchange ability and consequently a higher adsorption capacity. Also, the presence of more oxygen functional group (-OH groups) on the surface of $MgCl_2$ pretreated AC may enhance the Pb (II) adsorption capacity (Fig. 8) [12]. In comparison to other pretreatments of AC described before, Mg is thought to reflect more affinity towards Pb (II) which is attributed to its electronegativity and electric charge. The significant difference in the potential Pb (II) adsorption capacity of the prepared ACs could be attributed to the more electric charge of Ca and Mg (2+) than Na and K (1+) and higher electronegativity of Mg (1.31 Pauling) than Ca (1 Pauling). Finally, it can be said that $MgCl_2$ pretreated AC showed higher Pb (II) adsorption which is in good agreement with the study of Li et al. [65]. Furthermore, the treatment of biomass with ash increased significantly the Pb (II) adsorption capacity ($q_m = 1250.63$ mg g^{-1}, Table 4) due to its mineral contents such as Mg, Ca, Na and K. The use of ash for biomass pretreatment is considered value added and cost-effective. Ash pretreatment not only reduces the use of chemicals for biomass pretreatment but also manages the waste generated by lignocellulosic waste combustion.

Table 8
Desorption efficiency (%) of Pb (II) and Cr (VI) using 0.5 M of HCl and NaOH solution respectively.

Metal	Desorption efficiency (%)	
Pb (II)	Non-pretreated AC	91.2 ± 2.50
	$MgCl_2$-AC	99.5 ± 3.20
Cr (VI)	Non-pretreated AC	60.5 ± 2.01
	HCl-AC	56.8 ± 3.54

On the other hand, the Cr (VI) adsorption process is closely related to both microporous structure and functional groups [13]. Among the surface chemical and physical properties of ACs, the micropores play a key role in Cr (VI) adsorption capacity [10]. Therefore, the larger the ACs micropore volume, the greater the Cr (VI) adsorption capacity [66]. Similar observations were made by researchers while studying the preparation and application of microporous AC for the removal of Cr (VI) from aqueous phase [67,68]. These results are in good agreement with our study. The HCl pretreated AC had the highest surface area and micropore volume (Fig. 6 and Table 7) and achieved the highest Cr (VI) adsorption capacity (Table 4). Leaching pretreatment using water, HNO_3 and aquafortis seems to have a significant influence on the development of microporous structure and hence much greater Cr (VI) removal. Water treatment had a moderate effect on Cr (VI) adsorption capacity, possibly due to less removal of inorganic compared with HCl pretreatment [35]. Since HNO_3 is a strong oxidant and probably impact on the biomass structure [37], its effect on the AC modification was minimal. The Cr (VI) adsorption capacity of obtained pretreated ACs with alkali and alkali earth salts were relatively lower than non- pretreated ACs (Table 4) which might be attributed to the presence of mineral cations and hence decreased micropore fractions and creation of more mesopore fractions (Table 7).

4. Conclusion

In this work, ACs prepared from pretreated Elm tree sawdust were used for adsorption of Pb (II) and Cr (VI) from aqueous solution. Overall, the pretreatment with alkali and alkali earth metals improved the Pb (II) adsorption capacity. On the other hand, acid leaching of biomass provided an AC with high Cr (VI) adsorption capacity. The HCl-treated biomass resulted in a highly microporous AC with 0.443 cm^3 g^{-1} micropore volume and the maximum adsorption capacity of 190 mg g^{-1} for Cr (VI). Meanwhile, the $MgCl_2$-treatment extensively improved the mesoporosity to 0.347 cm^3 g^{-1} in comparison to 0.0761 cm^3 g^{-1} for non- treated AC. The adsorption capacity of Pb (II) was found to be 1430 mg g^{-1}. A pseudo-second order kinetic model explained well the Pb (II) and Cr (VI) adsorption process for the prepared ACs. The AC pretreated with $MgCl_2$ displayed a good correlation with the Langmuir isotherm model while the Temkin model exhibited a better fit to the Cr (VI) adsorption data. These results suggest that the development of porous structure (microporous or mesoporous fraction) of ACs through pretreatment may be an acceptable solution for efficient removal of Pb (II) and Cr (VI) from aqueous solutions. However, in practical point of view, the potential of reusability of the synthesized sorbents should be considered in future studies.

CRediT authorship contribution statement

Seyyedeh Maryam Kharrazi: Methodology, Formal analysis, Investigation, Writing original draft, Writing-review and editing.

Mohsen Soleimani: Conceptualization, Methodology, Resources, Validation, Writing original draft, Writing-review and editing, Supervision, Project administration, Funding acquisition.

Mojtaba Jokar: Investigation, Writing original draft, Writing-review and editing.

Tobias Richards: Validation, Resources, Writing-review and editing.

Anita Pettersson: Validation, Resources, Writing-review and editing.

Nourollah Mirghaffari*: Conceptualization, Methodology, Resources, Validation, Writing original draft, Writing-review and editing, Supervision, Project administration, Funding acquisition.

Appendix A. Supplementary data

Supplementary data to this article can be found online at https://doi.org/10.1016/j.ijbiomac.2021.03.078.

References

[1] Y. El Maguana, N. Elhadiri, M. Bouchdoug, M. Benchanaa, Study of the influence of some factors on the preparation of activated carbon from walnut cake using the fractional factorial design, Journal of Environmental Chemical Engineering 6 (1) (2018) 1093–1099.

[2] R. Li, J.J. Wang, L.A. Gaston, B. Zhou, M. Li, R. Xiao, Q. Wang, Z. Zhang, H. Huang, W. Liang, H. Huang, X. Zhang, An overview of carbothermal synthesis of metal–biochar composites for the removal of oxyanion contaminants from aqueous solution, Carbon 129 (2018) 674–687.

[3] K. Gupta, O.P. Khatri, Fast and efficient adsorptive removal of organic dyes and active pharmaceutical ingredient by microporous carbon: effect of molecular size and charge, Chem. Eng. J. 378 (2019), 122218, .

[4] A.I. Osman, J. Blewitt, J.K. Abu-Dahrieh, C. Farrell, A.A.H. Al-Muhtaseb, J. Harrison, D.W. Rooney, Production and characterisation of activated carbon and carbon nanotubes from potato peel waste and their application in heavy metal removal, Environ. Sci. Pollut. Res. 26 (36) (2019) 37228–37241.

[5] G. Özsin, M. Kılıç, E. Apaydın-Varol, A.E. Pütün, Chemically activated carbon production from agricultural waste of chickpea and its application for heavy metal adsorption: equilibrium, kinetic, and thermodynamic studies, Appl Water Sci 9 (3) (2019) 56–70.

[6] G.Z. Kyzas, E.A. Deliyanni, K.A. Matis, Activated carbons produced by pyrolysis of waste potato peels: cobalt ions removal by adsorption, Colloids Surf. A Physicochem. Eng. Asp. 490 (2016) 74–83.

[7] M. Riaz, R. Nadeem, M.A. Hanif, T.M. Ansari, K.-u. Rehman, Pb(II) biosorption from hazardous aqueous streams using Gossypium hirsutum (cotton) waste biomass, J. Hazard. Mater. 161 (1) (2009) 88–94.

[8] K. Mishima, X. Du, S. Sekiguchi, N. Kano, Experimental and theoretical studies on the adsorption and desorption mechanisms of chromate ions on cross-linked chitosan, Journal of Functional Biomaterials 8 (4) (2017) 51.

[9] A.A. Ensafi, M. Jokar, M. Ghiaci, Modified multiwall carbon nanotubes supported on graphite as a suitable solid nano-sorbent for selective separation and preconcentration of trace amounts of cadmium and lead ions, J. Iran. Chem. Soc. 12 (3) (2015) 457–467.

[10] S.M. Kharrazi, N. Mirghaffari, M.M. Dastgerdi, M. Soleimani, A novel post-modification of powdered activated carbon prepared from lignocellulosic waste through thermal tension treatment to enhance the porosity and heavy metals adsorption, Powder Technol. 366 (2020) 358–368.

[11] M. Danish, T. Ahmad, A review on utilization of wood biomass as a sustainable precursor for activated carbon production and application, Renew. Sust. Energ. Rev. 87 (2018) 1–21.

[12] L.-L. Ling, W.-J. Liu, S. Zhang, H. Jiang, Magnesium oxide embedded nitrogen self-doped biochar composites: fast and high-efficiency adsorption of heavy metals in an aqueous solution, Environ. Sci. Technol. 51 (17) (2017) 10081–10089.

[13] S.-J. Park, Y.-S. Jang, Pore structure and surface properties of chemically modified activated carbons for adsorption mechanism and rate of Cr(VI), J. Colloid Interface Sci. 249 (2002) 458–463.

[14] J. Acharya, U. Kumar, M.P. Rafi, Removal of heavy metal ions from wastewater by chemically modified agricultural waste material as potential adsorbent-a review, International Journal of Current Engineering and Technology 8 (3) (2018) 526–530.

[15] F. Ahmad, W.M.A.W. Daud, M.A. Ahmad, R. Radzi, The effects of acid leaching on porosity and surface functional groups of cocoa (Theobroma cacao)-shell based activated carbon, Chem. Eng. Res. Des. 91 (6) (2013) 1028–1038.

[16] S.V. Novais, M.D.O. Zenero, J. Tronto, R.F. Conz, C.E.P. Cerri, M. Açıkyıldız, Poultry manure and sugarcane straw biochars modified with $MgCl_2$ for phosphorus adsorption, J. Environ. Manag. 214 (2018) 36–44.

[17] A. Moazzam, N. Jamil, F. Nadeem, A. Qadir, M. Zameer, N. Ahsan, Reactive dye removal by a novel biochar/ MgO nanocomposite, J. Chem. Soc. Pak. 39 (1) (2017) 26–34.

[18] Z. Yuan, Z. Xu, D. Zhang, W. Chen, T. Zhang, Y. Huang, L. Gu, H. Deng, D. Tian, Box-Behnken design approach towards optimization of activated carbon synthesized by co-pyrolysis of waste polyester textiles and MgCl2, Appl. Surf. Sci. 427 (2018) 340–348.

[19] R. Bodirlau, I. Spiridon, C.A. Teaca, Chemical investigation on wood tree species in a temperate forest, East-Northern Romania, Bioresources 2 (1) (2007) 41–57.

[20] M. Tüzen, Determination of heavy metals in soil, mushroom and plant samples by atomic absorption spectrometry, Microchem. J. 74 (3) (2003) 289–297.

[21] E. Daneshvar, A. Vazirzadeh, A. Niazi, M. Kousha, M. Naushad, A. Bhatnagar, Desorption of methylene blue dye from brown macroalga: effects of operating parameters, isotherm study and kinetic modeling, J. Clean. Prod. 152 (2017) 443–453.

[22] Y. Wang, J. Pan, Y. Li, P. Zhang, M. Li, H. Zheng, X. Zhang, H. Li, Q. Du, Methylene blue adsorption by activated carbon, nickel alginate/activated carbon aerogel, and nickel alginate/graphene oxide aerogel: a comparison study, Journal of Materials Research and Technology 9 (6) (2020) 12443–12460.

[23] P. Zong, D. Cao, Y. Cheng, S. Wang, J. Zhang, Z. Guo, T. Hayat, N.S. Alharbi, C. He, Carboxymethyl cellulose supported magnetic graphene oxide composites by plasma induced technique and their highly efficient removal of uranium ions, Cellulose 26 (6) (2019) 4039–4060.

[24] M. Ghasemi, M. Zeinaly Khosroshahy, A. Bavand Abbasabadi, N. Ghasemi, H. Javadian, M. Fattahi, Microwave-assisted functionalization of Rosa Canina-L fruits activated carbon with tetraethylenepentamine and its adsorption behavior toward Ni(II) in aqueous solution: kinetic, equilibrium and thermodynamic studies, Powder Technol. 274 (2015) 362–371.

[25] X. Huang, X. Zhan, C. Wen, F. Xu, L. Luo, Amino-functionalized magnetic bacterial cellulose/activated carbon composite for Pb2+ and methyl orange sorption from aqueous solution, J. Mater. Sci. Technol. 34 (5) (2018) 855–863.

[26] Q. Miao, Y. Tang, J. Xu, X. Liu, L. Xiao, Q. Chen, Activated carbon prepared from soybean straw for phenol adsorption, J. Taiwan Inst. Chem. Eng. 44 (2013) 458–465.

[27] K.Y. Foo, B.H. Hameed, Insights into the modeling of adsorption isotherm systems, Chem. Eng. J. 156 (1) (2010) 2–10.

[28] S.A. Dastgheib, J. Ren, M. Rostam-Abadi, R. Chang, Preparation of functionalized and metal-impregnated activated carbon by a single-step activation method, Appl. Surf. Sci. 290 (2014) 92–101.

[29] V. Sricharoenchaikul, C. Pechyen, D. Aht-ong, D. Atong, Preparation and characterization of activated carbon from the pyrolysis of physic nut (Jatropha curcas L.) waste, Energy Fuel 22 (2008) 31–37.

[30] A. Heidari, H. Younesi, A. Rashidi, A. Ghoreyshi, Adsorptive removal of CO_2 on highly microporous activated carbon prepared from Eucalyptus camaldulensis wood: effect of chemical activation, J. Taiwan Inst. Chem. Eng. 45 (2014) 579–588.

[31] X. Gao, L. Wu, Z. Li, Q. Xu, W. Tian, R. Wang, Preparation and characterization of high surface area activated carbon from pine wood sawdust by fast activation with H 3 PO 4 in a spouted bed, Journal of Material Cycles and Waste Management 20 (2) (2018) 925–936.

[32] C.A. Demarchi, B.S. Michel, N. Nedelko, A. Ślawska-Waniewska, P. Dłużewski, A. Kaleta, R. Minikayev, T. Strachowski, L. Lipińska, J. Dal Magro, C.A. Rodrigues, Preparation, characterization, and application of magnetic activated carbon from termite feces for the adsorption of Cr(VI) from aqueous solutions, Powder Technol. 354 (2019) 432–441.

[33] B. Cagnon, X. Py, A. Guillot, F. Stoeckli, G. Chambat, Contributions of hemicellulose, cellulose and lignin to the mass and the porous properties of chars and steam activated carbons from various lignocellulosic precursors, Bioresour. Technol. 100 (1) (2009) 292–298.

[34] M. Açıkyıldız, A. Gürses, S. Karaca, Preparation and characterization of activated carbon from plant wastes with chemical activation, Microporous Mesoporous Mater. 198 (2014) 45–49.

[35] P. Das, A. Ganesh, P. Wangikar, Influence of pretreatment for deashing of sugarcane bagasse on pyrolysis products, Biomass Bioenergy 27 (5) (2004) 445–457.

[36] B.M. Jenkins, R.R. Bakker, J.B. Wei, On the properties of washed straw, Biomass Bioenergy 10 (4) (1996) 177–200.

[37] V. Datsyuk, M. Kalyva, K. Papagelis, J. Parthenios, D. Tasis, A. Siokou, I. Kallitsis, C. Galiotis, Chemical oxidation of multiwalled carbon nanotubes, Carbon 46 (2008) 833–840.

[38] D. Carpenter, T.L. Westover, S. Czernik, W. Jablonski, Biomass feedstocks for renewable fuel production: a review of the impacts of feedstock and pretreatment on the yield and product distribution of fast pyrolysis bio-oils and vapors, Green Chem. 16 (2) (2014) 384–406.

[39] P.R. Patwardhan, R.C. Brown, B.H. Shanks, Product distribution from the fast pyrolysis of hemicellulose, ChemSusChem 4 (5) (2011) 636–643.

[40] A. Şencan, M. Karaboyacı, M. Kılıç, Determination of lead(II) sorption capacity of hazelnut shell and activated carbon obtained from hazelnut shell activated with $ZnCl_2$, Environ. Sci. Pollut. Res. 22 (2015) 3238–3248.

[41] C. Valderrama, X. Gamisans, X. de las Heras, A. Farrán, J.L. Cortina, Sorption kinetics of polycyclic aromatic hydrocarbons removal using granular activated carbon: Intraparticle diffusion coefficients, J. Hazard. Mater. 157 (2) (2008) 386–396.

[42] K. Mohanty, D. Das, M.N. Biswas, Adsorption of phenol from aqueous solutions using activated carbons prepared from Tectona grandis sawdust by ZnCl2 activation, Chem. Eng. J. 115 (1) (2005) 121–131.

[43] M. Lesaoana, R.P.V. Mlaba, F.M. Mtunzi, M.J. Klink, P. Ejidike, V.E. Pakade, Influence of inorganic acid modification on Cr(VI) adsorption performance and the physicochemical properties of activated carbon, South African Journal of Chemical Engineering 28 (2019) 8–18.

[44] X. Zhang, L. Lv, Y. Qin, M. Xu, X. Jia, Z. Chen, Removal of aqueous Cr(VI) by a magnetic biochar derived from Melia azedarach wood, Bioresour. Technol. 256 (2018) 1–10.

[45] O. Hamdaoui, E. Naffrechoux, Modeling of adsorption isotherms of phenol and chlorophenols onto granular activated carbon: part I. two-parameter models and equations allowing determination of thermodynamic parameters, J. Hazard. Mater. 147 (1) (2007) 381–394.

[46] I.D. Mall, V.C. Srivastava, N.K. Agarwal, I.M. Mishra, Removal of Congo red from aqueous solution by bagasse fly ash and activated carbon: kinetic study and equilibrium isotherm analyses, Chemosphere 61 (4) (2005) 492–501.

[47] E.M. Mistar, T. Alfatah, M.D. Supardan, Synthesis and characterization of activated carbon from Bambusa vulgaris striata using two-step KOH activation, Journal of Materials Research and Technology 9 (3) (2020) 6278–6286.

[48] K. Fu, Q. Yue, A. Gao, Y. Wang, Q. Li, Activated carbon from tomato stem by chemical activation with FeCl2, Colloids and Surfaces A 529 (2017) 842–849.

[49] G.-G. Choi, S.-H. Jung, S.-J. Oh, J.-S. Kim, Total utilization of waste tire rubber through pyrolysis to obtain oils and CO2 activation of pyrolysis char, Fuel Process. Technol. 123 (2014) 57–64.

[50] E.L.K. Mui, W.H. Cheung, M. Valix, G. McKay, Dye adsorption onto activated carbons from Tyre rubber waste using surface coverage analysis, J. Colloid Interface Sci. 347 (2) (2010) 290–300.

[51] X. Zhang, S. Zhang, H. Yang, J. Shao, Y. Chen, Y. Feng, X. Wang, H. Chen, Effects of hydrofluoric acid pre-deashing of rice husk on physicochemical properties and

CO2 adsorption performance of nitrogen-enriched biochar, Energy 91 (2015) 903–910.
[52] P. Yu, Y. Xue, F. Gao, Z. Liu, X. Cheng, K. Yang, Phosphorus removal from aqueous solution by pre- or post-modified biochars derived from agricultural residues, Water Air Soil Pollut. 227 (10) (2016), 370, .
[53] Z. Yuan, Z. Xu, D. Zhang, W. Chen, Y. Huang, T. Zhang, D. Tian, H. Deng, Y. Zhou, Z. Sun, Mesoporous activated carbons synthesized by pyrolysis of waste polyester textiles mixed with mg-containing compounds and their Cr(VI) adsorption, Colloids and Surfaces A 549 (2018) 86–93.
[54] W.-J. Liu, H. Jiang, K. Tian, Y.-W. Ding, H.-Q. Yu, Mesoporous carbon stabilized MgO nanoparticles synthesized by pyrolysis of MgCl2 preloaded waste biomass for highly efficient CO2 capture, Environ. Sci. Technol. 47 (16) (2013) 9397–9403.
[55] T. Morishita, Y. Soneda, T. Tsumura, M. Inagaki, Preparation of porous carbons from thermoplastic precursors and their performance for electric double layer capacitors, Carbon 44 (2006) 2360–2367.
[56] H. Konno, H. Onishi, N. Yoshizawa, K. Azumi, MgO-templated nitrogen-containing carbons derived from different organic compounds for capacitor electrodes, J. Power Sources 195 (2010) 667–673.
[57] R.H. Hesas, A. Arami-Niya, W.M.A.W. Daud, J.N. Sahu, Comparison of oil palm shell-based activated carbons produced by microwave and conventional heating methods using zinc chloride activation, J. Anal. Appl. Pyrolysis 104 (2013) 176–184.
[58] C.K. Rojas-Mayorga, A. Bonilla-Petriciolet, I.A. Aguayo-Villarreal, V. Hernández-Montoya, M.R. Moreno-Virgen, R. Tovar-Gómez, M.A. Montes-Morán, Optimization of pyrolysis conditions and adsorption properties of bone char for fluoride removal from water, J. Anal. Appl. Pyrolysis 104 (2013) 10–18.
[59] A.R. Tobi, J.O. Dennis, H.M. Zaid, A.A. Adekoya, A. Yar, U. Fahad, Comparative analysis of physiochemical properties of physically activated carbon from palm bio-waste, Journal of Materials Research and Technology 8 (5) (2019) 3688–3695.
[60] S. Mopoung, P. Moonsri, W. Palas, S. Khumpai, Characterization and properties of activated carbon prepared from tamarind seeds by KOH activation for Fe(III) adsorption from aqueous solution, Sci. World J. 2015 (2015) 1–9.
[61] J. Hu, G. Chen, I.M.C. Lo, Removal and recovery of Cr(VI) from wastewater by maghemite nanoparticles, Water Res. 39 (2005) 4528–4536.
[62] C. Fang, T. Zhang, P. Li, R. Jiang, S. Wu, H. Nie, Y. Wang, Phosphorus recovery from biogas fermentation liquid by Ca–mg loaded biochar, J. Environ. Sci. 29 (2015) 106–114.
[63] Z. Hu, L. Lei, Y. Li, Y. Ni, Chromium adsorption on high-performance activated carbons from aqueous solution, Sep. Purif. Technol. 31 (2003) 13–18.
[64] T.Z. Ci Fang, P. Li, R.-F. Jiang, Y.-C. Wang, Application of magnesium modified corn biochar for phosphorus removal and recovery from swine wastewater, Int. J. Environ. Res. Public Health 11 (2005) 9217–9237.
[65] K. Li, Y. Jiang, X. Wang, D. Bai, H. Li, Z. Zheng, Effect of nitric acid modification on the lead(II) adsorption of mesoporous biochars with different mesopore size distributions, Clean Techn. Environ. Policy 18 (3) (2016) 797–805.
[66] Z. Hu, L. Lei, Y. Li, Y. Ni, Chromium adsorption on high-performance activated carbons from aqueous solution, Sep. Purif. Technol. 31 (1) (2003) 13–18.
[67] R. Gottipati, S. Mishra, Preparation of microporous activated carbon from Aegle Marmelos fruit shell and its application in removal of chromium(VI) from aqueous phase, J. Ind. Eng. Chem. 36 (2016) 355–363.
[68] R. Gottipati, S. Mishra, Process optimization of adsorption of Cr(VI) on activated carbons prepared from plant precursors by a two-level full factorial design, Chem. Eng. J. 160 (1) (2010) 99–107.